

DTIC FILE COPY

(2)

RADC-TR-89-264
In-House Report
October 1989

AD-A226 218



INVESTIGATION OF A BENT WIRE CHIRAL: ELECTROMAGNETIC SCATTERING

Allan C. Buck

DTIC
ELECTE
SEP 07 1990
S D U D

APPROVED FOR PUBLIC RELEASE; DISTRIBUTION UNLIMITED.

ROME AIR DEVELOPMENT CENTER
Air Force Systems Command
Griffiss Air Force Base, NY 13441-5700

90 09 06 012

This report has been reviewed by the RADC Public Affairs Office (PA) and is releasable to the National Technical Information Service (NTIS). At NTIS it will be releasable to the general public, including foreign nations.

RADC TR-89-264 has been reviewed and is approved for publication.

APPROVED:



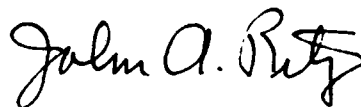
J. LEON POIRIER
Chief, Applied Electromagnetics Division
Directorate of Electromagnetics

APPROVED:



JOHN K. SCHINDLER
Director of Electromagnetics

FOR THE COMMANDER:



JOHN A. RITZ
Directorate of Plans and Programs

If your address has changed or if you wish to be removed from the RADC mailing list, or if the addressee is no longer employed by your organization, please notify RADC (EECT) Hanscom AFB MA 01731-5000. This will assist us in maintaining a current mailing list.

Do not return copies of this report unless contractual obligations or notices on a specific document requires that it be returned.

REPORT DOCUMENTATION PAGE

Form Approved
OMB No. 0704-0188

Public reporting for this collection of information is estimated to average 1 hour per response, including the time for reviewing instructions, searching existing data sources, gathering and maintaining the data needed, and completing and reviewing the collection of information. Send comments regarding this burden estimate or any other aspect of this collection of information, including suggestions for reducing this burden, to Washington Headquarters Services, Directorate for Information Operations and Reports, 1215 Jefferson Davis Highway, Suite 1204, Arlington, VA 22202-4302, and to the Office of Management and Budget, Paperwork Reduction Project (0704-0188), Washington, DC 20503.

1. AGENCY USE ONLY (Leave blank)		2. REPORT DATE 19 Oct 89	3. REPORT TYPE AND DATES COVERED In-House Jul 88 - Jun 89	
4. TITLE AND SUBTITLE Investigation of a Bent Wire Chiral; Electromagnetic Scattering			5. FUNDING NUMBERS PE 62702F PR 4600 TA 15 WU 06	
6. AUTHOR(S) Buck, Allan C.				
7. PERFORMING ORGANIZATION NAME(S) AND ADDRESS(ES) Rome Air Development Center RADC/EECT Hanscom AFB Massachusetts 01731-5000			8. PERFORMING ORGANIZATION REPORT NUMBER RADC-TR-89-264	
9. SPONSORING/MONITORING AGENCY NAME(S) AND ADDRESS(ES)			10. SPONSORING/MONITORING AGENCY REPORT NUMBER	
11. SUPPLEMENTARY NOTES				
12a. DISTRIBUTION/AVAILABILITY STATEMENT Approved for public release; distribution unlimited.			12b. DISTRIBUTION CODE	
13. ABSTRACT (Maximum 200 words) The bistatic scattering from a bent wire chiral has been analyzed and a computer modeling capability has been developed. A simple model was also developed to aid in interpreting the chiral body's scattering. Behavior of the scattered fields was investigated as the chiral's geometry was varied. Data was presented that would be useful in the design of chiral media.				
14. SUBJECT TERMS Scattering, Chiral, Wire Scatterer, Moment Method, RFA			15. NUMBER OF PAGES 36	
			16. PRICE CODE	
17. SECURITY CLASSIFICATION OF REPORT UNCLASSIFIED	18. SECURITY CLASSIFICATION OF THIS PAGE UNCLASSIFIED	19. SECURITY CLASSIFICATION OF ABSTRACT UNCLASSIFIED	20. LIMITATION OF ABSTRACT SAR	

Contents

1. INTRODUCTION	1
2. NUMERICAL METHODS	5
3. SOME SIMPLE EXPECTATIONS	9
4. RESULTS	13
5. CONCLUSIONS	28
REFERENCES	29



Accession For	
NTIS CRA&I	<input checked="" type="checkbox"/>
DTIC TAB	<input type="checkbox"/>
Unannounced	<input type="checkbox"/>
Justification	
By	
Distribution /	
Availability Codes	
Dist	Avail and/or Special
A-1	

Illustrations

1.	Helix-Dipole Chiral Geometry	3
2.	Comparison of a Chiral with its Image	4
3.	Flow Diagram of Chiral	10
4.	3-D Plot Showing Scattering Dependence on Loop Diameter, Vertical Cut	15
5.	3-D Plot Showing Scattering Dependence on Loop Diameter, Horizontal Cut	16
6.	3-D Plot Showing Scattering Dependence on Dipole Length, Vertical Cut	18
7.	3-D Plot Showing Scattering Dependence on Dipole Length, Horizontal Cut	19
8.	3-D Plot Showing Scattering Dependence on Dipole Feed Position, Vertical Cut	21
9.	3-D Plot Showing Scattering Dependence on Dipole Feed Position, Horizontal Cut	22
10.	3-D Plot Showing Scattering Dependence on Illumination for Variations of Theta, Vertical Cut	24
11.	3-D Plot Showing Scattering Dependence on Illumination for Variations of Theta, Horizontal Cut	25
12.	3-D Plot Showing Scattering Dependence on Illumination for Variation of Phi, Vertical Cut	26

13.	3-d Plot Showing Scattering Dependence on Illumination for Variation of Phi, Horizontal Cut	27
-----	--	----

Investigation of a Bent Wire Chiral; Electromagnetic Scattering

1. INTRODUCTION

Chiral media have recently attracted attention in the electromagnetics field due to their transmission and scattering properties. Several authors have reported interesting results concerning the use of chiral media as polarization rotators. In the most recent reports, the authors have assumed a suitable chiral body exists and then proceeded to derive constitutive relationships, dyadic Green's functions, and indices of chirality.^{1,2,3} Using the relationships derived, one may predict the macroscopic behavior

(Received for publication 14 November 1989)

¹ Jaggard, D.L., Mickelson, A.R., and Papas, C.H. (1979) On Electromagnetic Waves in Chiral Media, *Applied Physics*, New York: Springer Verlag, 18: 211-216.

² Lakhtakia, A., Varadan, V.V., and Varadan, V.K. (1986) A parametric study of microwave reflection characteristics of a planar achiral-chiral interface, *IEEE Transactions on Electromagnetic Compatibility*, EMC-28 (No. 2): 90-95.

³ Bassiri, S., Engheta, N., and Papas, C.H. (1986) Dyadic Green's function and dipole radiation in chiral media, *Alta Frequenza*, LV (No 2): 83-88.

of a chiral media. The intent of this study was to investigate some form of a simple chiral body that may be suitable as an element in a chiral medium. An easily realized chiral body made from a bent wire was chosen for its simplicity in modeling and fabrication. Before describing the bent wire geometry used, a digression will be made to define exactly what is meant by a body being chiral.

A chiral body is defined as any body that cannot be brought into congruence with its image by simple rotation and translation. Chirality is a geometric property that is quite common in such everyday items as screws, helices, and hands. The word chiral is derived from the Greek word for hand, cher- or cheiro-, therefore chirals can be assigned some handed sense. Helices are considered to be right-handed or left-handed depending on their winding sense. From our experience with helical antennas we know these structures interact differently with right-hand or left-hand elliptically polarized waves and, therefore, are chiral. This chirality is used in a chiral medium to control its polarization dependence or handedness. With this definition in mind a simple chiral body was chosen. The chiral of interest was constructed by connecting a dipole antenna to a short helix segment, as shown in Figure 1. By comparing the two bent wire chirals of Figure 2, a distinct difference can be seen in their winding sense. These two chirals are images of each other.

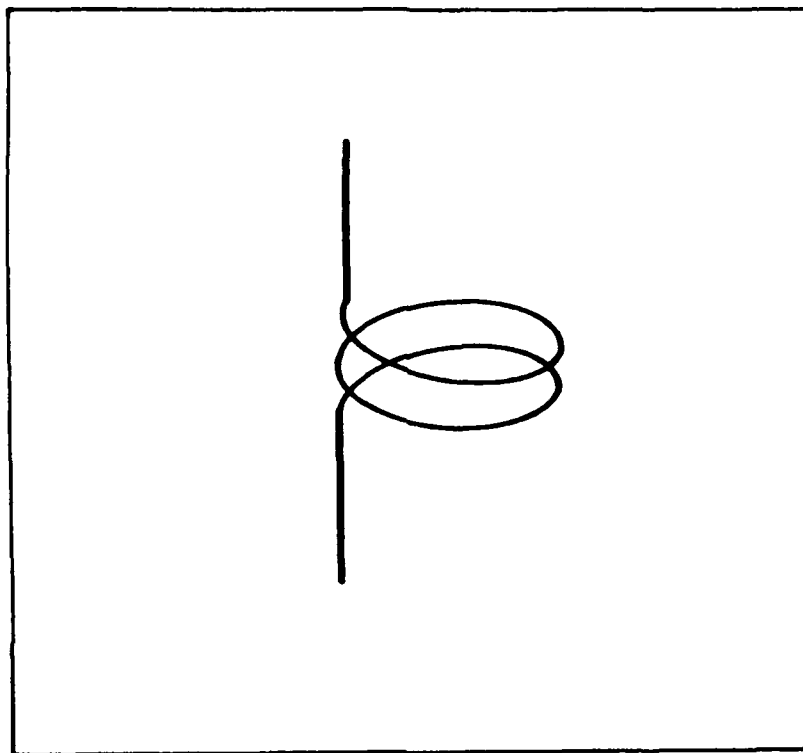


Figure 1. Dipole-Helix Chiral Consisting of a Two Turn Helix With Two Straight Wire Segments Attached to its Top and Bottom.

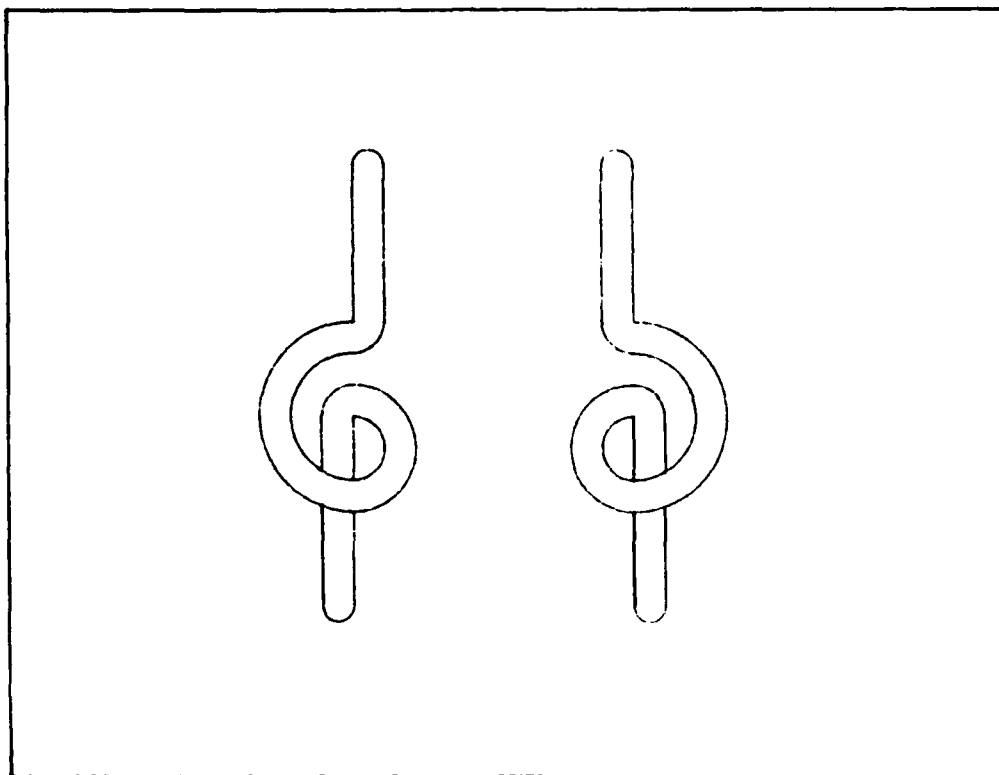


Figure 2. Two Bent Wire Chirals, (a) is a Left-Handed Chiral and (b) is its Image, Which is a Right-Handed Chiral.

Chiral media have some interesting electromagnetic properties that make them quite useful in many engineering applications. In a chiral medium the electric and magnetic fields are coupled via an index of chirality. Advantage can be taken of this interdependence to create a material that behaves, in some ways, similar to a ferrite, rotating the polarization vector of an electromagnetic wave propagating through it. Unlike a ferrite, a chiral material's rotation does not depend on the direction of propagation. Chiral media have many potential uses such as frequency selective surfaces, polarization selective surfaces, and microwave circuit devices. To implement these applications a good understanding of the tuning characteristics and dynamic range available from a given chiral was required. Control of the chiral medium's macroscopic performance depends on the characteristics of the individual chirals. The rest of this report addresses electromagnetic scattering from a simple bent wire chiral and the analytical methods used to predict its behavior.

2. NUMERICAL METHODS

The dipole-helix chiral is a simple bent wire structure. This geometry is very well suited to a method of moments solution for its scattered electromagnetic fields. The general method of moments involves solving equations of the form

$$\mathcal{L}(f) = g \tag{1}$$

where $\mathcal{L}(f)$ is a linear operator on f , the unknown function, that yields the known excitation g .⁴ The unknown function may be expanded as a sum of basis functions.

$$f = \sum_n \alpha_n f_n \tag{2}$$

⁴ Harrington, R.F. (1968) *Field Computation by Moment Methods*, Malabar, Florida: Robert E. Krieger Publishing Company, pp. 1-7.

Using this representation for f , Eq. (1) may be rewritten as

$$\sum_n \alpha_n \mathcal{L}(f_n) = g. \quad (3)$$

Defining an appropriate inner product and applying it to both sides of Eq. (3) with the weighting function ω_m , we obtain

$$\sum_n \alpha_n \langle \omega_m, \mathcal{L}(f_n) \rangle = \langle \omega_m, g \rangle. \quad (4)$$

Equation (4) may now be cast in matrix form as

$$[l_{mn}] [\alpha_n] = [g_m] \quad (5)$$

which may yield an exact solution depending on the choice of f_n and ω_m .

Applying the above general method of moments, herein referred to as MOM, to the wire scattering problem involves solving the electric field integral equation

$$E(r) = \frac{-j\eta}{4\pi k} \iiint_{V'} J(r') \bar{G}(r, r') dV' \quad (6)$$

where the volume current $J(r')$ is unknown and the field, $E(r)$, is known at the wire scatterer's surface by application of the boundary conditions.⁵ The dyadic Green's function

$$\bar{G}(r, r') = (k^2 \bar{I} + \nabla \nabla) g(r, r') \quad (7)$$

⁵ Burke, G.J. and Poggio, A.J. (1980) *Numerical Electric Magnetics Code (NEC)-Method of Moments, Vol 1, Part 1*, San Diego, CA, Naval Ocean Systems Command, pp. 3-5.

$$g(\mathbf{r}, \mathbf{r}') = \exp\left(\frac{-jk|\mathbf{r} - \mathbf{r}'|}{|\mathbf{r} - \mathbf{r}'|}\right) \quad (8)$$

is used for compactness of notation. The volume integral (Eq. (6)) may be written as

$$\mathbf{E}(\mathbf{r}) = \frac{-j\eta}{4\pi k} \iint_S \mathbf{J}_s(\mathbf{r}') \bar{\mathbf{G}}(\mathbf{r}, \mathbf{r}') dS' \quad (9)$$

for a perfect electric conductor, where the integral is evaluated over the surface of the wire and \mathbf{r} does not equal \mathbf{r}' . The singularity occurring at \mathbf{r} equal \mathbf{r}' may be eliminated by taking the limit of $\mathbf{E}(\mathbf{r})$ as \mathbf{r} approaches \mathbf{r}' . This yields the principal value integral.⁶

$$\mathbf{E}(\mathbf{r}) = \frac{-j\eta}{4\pi k} \oint \mathbf{J}_s(\mathbf{r}') \bar{\mathbf{G}}(\mathbf{r}, \mathbf{r}') dS' \quad (10)$$

This integral may be reduced to a scalar integral equation if several assumptions are made. For the geometries considered in this study the surface, S , is that of a cylindrical thin wire. The surface current, $\mathbf{J}_s(\mathbf{r})$, may be replaced by a current filament I . Then

$$I(s) \hat{\mathbf{s}} = 2\pi a \mathbf{J}_s(s) \quad (11)$$

where s is the distance parameter along the the wire and $\hat{\mathbf{s}}$ is a unit vector tangent to the wire axis at \mathbf{r} . The electric field integral equation may now be written as

$$\mathbf{E}(\mathbf{r}) = \frac{-j\eta}{4\pi k} \int I(s') (\mathbf{k}^2 \hat{\mathbf{s}} - \nabla \frac{\delta}{\delta s'}) g(\mathbf{r}, \mathbf{r}') ds'. \quad (12)$$

⁶ Poggio, A.J. and Miller, E.K. (1973) Integral Equation Solutions of Three Dimensional Scattering Problems, Chapt IV in *Computer Techniques for Electromagnetics*, Edited by R. Mittra, New York: Pergamon Press.

Invoking the boundary condition $E_{\tan} = 0$, allows us to write

$$\hat{n}(r) \times [E^s(r) + E^i(r)] = 0, \quad (13)$$

where E^s and E^i are the scattered and incident electric fields, respectively. Then using Eq. (12) for the scattered field and enforcing Eq. (13) at the wire surface we may write

$$-\hat{s} \cdot E^i = \frac{-j\eta}{4\pi k} \int_L I(s') \left(k^2 \hat{s} \cdot \hat{s}' - \frac{\delta}{\delta s \delta s'} \right) g(r, r') ds' \quad (14)$$

Equation (14) is a scalar equation for the total field at the wire surface.

Having derived the integral equation for the total electric field at the wire's surface, the MOM may be applied. The linear operator $\mathcal{L}(f)$ is the integral of Eq. (14)

$$\mathcal{L}(I(s)) = \frac{-j\eta}{4\pi k} \int_L I(s') \left(k^2 \hat{s} \cdot \hat{s}' - \frac{\delta}{\delta s \delta s'} \right) g(r, r') ds' \quad (15)$$

$$g(r, r') = \hat{s} \cdot E^i(r). \quad (16)$$

Expanding the unknown currents in a linear sum of a constant term and two piecewise sinusoidal terms yields

$$I_n(s) = A_n + B_n \sin k(s-s_n) + C_n \cos k(s-s_n) \quad (17)$$

$$|s-s_n| < \frac{\Delta_n}{2} \quad (18)$$

where Δ_n is the segment length. The three coefficients, A_n , B_n , and C_n in Eq. (17), are related to each other by local boundary conditions imposed on the segments and can be

treated as one unknown coefficient, which is derived in detail in Reference 5 but is omitted for the sake of brevity. Using this information, the current can be represented in the desired format as

$$I(s) \approx \sum_n^N \alpha_n f_n(s). \quad (19)$$

Finally, an appropriate weighting function and an appropriate inner product must be chosen. The inner product of the functions f and g is defined as

$$\langle f, g \rangle = \int_s f(r)g(r)ds. \quad (20)$$

In order to minimize the requisite computation time the Dirac Delta function, $\omega_m = \delta(r-r_m)$, was used for the weighting function. By nature of the Dirac Delta function's sampling property, the inner product integral is reduced to a simple calculation at the sample point, that is point matching.

The MOM numerical computations as outlined here were performed using the Numerical Electromagnetics Code (NEC) on a VAX 11-750. Due to the nature of this study, with its extensive parameter variations, an ensemble of computer programs were developed to minimize the time required to generate, analyze and plot large numbers of test cases. This involved modification of the NEC code, creation of an input file generator, and writing several plotting routines.

3. SOME SIMPLE EXPECTATIONS

The purpose of this study was to investigate the behavior of a chiral body. Having chosen the dipole-helix combination for its simplicity, some simple expectations were hypothesized with regards to the chiral's scattering characteristics. For this study the helix section had very little pitch angle and, therefore, was virtually flat allowing it to be treated as a loop antenna. Conceptually, the chiral was modeled as a combination of two linear antenna elements connected at their terminal nodes. The total response of the combination was therefore predicted from the responses of its constituent parts. This was merely an application of linear network theory. Both the loop and dipole antenna's

scattering and radiation behavior are well understood, which allowed some expectations and conclusions to be formed concerning the chiral's scattering behavior.

With the two antennas aligned as in Figure 1, they should be principally coupled by their terminals. This was due to the two antenna polarization vectors being orthogonal. Loop antennas may be considered as magnetic dipoles⁷ and are, therefore, the dual of an electric dipole. Using this analogy the chiral can be treated as an electric dipole receiving a signal and in turn driving a loop as a transmitter (vertical polarization). Similarly the loop antenna may be considered to be receiving and in turn driving the dipole antenna as a transmitter (horizontal polarization). Figure 3 is a flow diagram depicting this arrangement, where the input and output terminals are considered at some incidence angle and scatter angle. The flow diagram assumes the dipole and helix may be characterized by a two port scattering matrix [S].

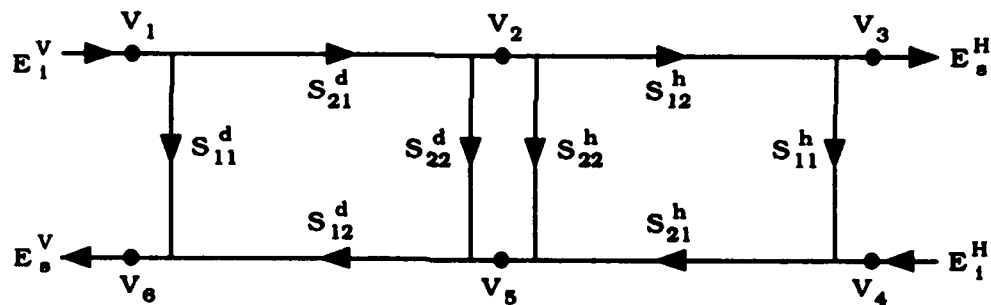


Figure 3. Flow Graph Representation of the Dipole Helix Combination. Scattering parameters, S, are shown with superscripted d for the dipole segment and superscripted h for the helix. Incident and scattered waves, E, are denoted by subscripted i and s respectively, while the polarization dependence is indicated by the superscripted H and V for horizontal and vertical.

⁷ Harrington, R.F. (1961) *Time-Harmonic Electromagnetic Fields*, New York; McGraw-Hill Book Co.

Using flow graph techniques, signal values at the output nodes V_6 , V_3 defined in Figure 3 may be related to the incident fields E_1^V , E_1^H , which represent the vertical and horizontal polarization components respectively. Beginning with the dipole's and helix's terminal junction we may write

$$V_2 = V_1 S_{21}^d + V_5 S_{22}^d \quad (21)$$

$$V_5 = V_4 S_{21}^h + V_2 S_{22}^h \quad (22)$$

Solving these two equations for nodes V_2 , V_5 we obtain

$$V_2 = \frac{V_1 S_{21}^d + S_{22}^d V_4 S_{21}^h}{1 - S_{22}^d S_{22}^h} \quad (23)$$

$$V_5 = \frac{V_4 S_{21}^h + S_{22}^h V_1 S_{21}^d}{1 - S_{22}^d S_{22}^h} \quad (24)$$

Scattered signals are determined from the output node voltage values which are given by

$$V_6 = V_1 S_{11}^d + V_5 S_{12}^d \quad (25)$$

$$V_3 = V_2 S_{12}^h + V_4 S_{11}^h \quad (26)$$

Substituting Eqs. (23) and (24) for V_2 , V_5 in Eqs. (25) and (26) and rearranging yields

$$V_3 = \frac{V_1 S_{21}^d S_{12}^h + V_4 (S_{22}^d S_{21}^h S_{12}^h + S_{11}^h (1 - S_{22}^h S_{22}^d))}{1 - S_{22}^h S_{22}^d} \quad (27)$$

$$V_6 = \frac{V_1(S_{22}^h S_{21}^d S_{12}^d + S_{11}^d (1 - S_{22}^h S_{22}^d)) + V_4 S_{21}^h S_{12}^d}{1 - S_{22}^h S_{22}^d} \quad (28)$$

From the flow graph we see that the node voltages V_3 and V_6 correlate to the scattered fields E_s^H and E_s^V . From Eqs. (27) and (28) we see the dipole-helix chiral will have components in both vertical and horizontal polarizations, thereby scattering, in general, an elliptically polarized wave for a given linearly polarized incident field.

The scattered wave parameters, such as axial ratio or tilt angle, may be adjusted provided there is sufficient robustness built into the chiral's component antennas. Tuning was accomplished by varying the constituent antenna's S-parameters. Some physical significance can be associated with the S-parameters by assuming: S_{22} was the antenna's terminal reflection coefficient, S_{11} was thought of as the antenna's structural mode reflection coefficient, and the transverse terms, S_{12} and S_{21} , were considered as the antenna's transmission efficiency. These S-parameters are all dependent on an antenna's geometry and environment. Geometric parameter variations on the chiral geometry have yielded some guidelines and limits as to the amount of tuning and control available from this particular chiral.

Separating the two antennas and treating them independently allowed for calculation of input impedances. The terminal impedance of these wire antennas is well documented in the literature.^{8,9} Solution methods employed by the NEC code are also capable of making these calculations. Terminal coupling between the dipole and loop antennas would be governed by the impedance match "seen" by the receiving antenna. This terminal loading also influenced the re-radiation, and the co-polarized radar cross section, significantly. Studying the terminal impedances of the two antennas and determining ways to adjust them illustrated what parameters should be varied to adjust the chiral's scattering behavior.

⁸ Harrison, C.W. and King, R.W.P. (1969) *Antennas and Waves: A Modern Approach*, Cambridge: MIT Press, pp. 539-569.

⁹ Stutzman, W.L. and Thiele, G.A. (1981) *Antenna Theory and Design*, New York: John Wiley & Sons, pp. 193-203.

4. RESULTS

As a precursor to all subsequent discussion, the bistatic scattering characteristics of the bodies of interest are in the far field and in what will be defined as the two principal planes. The principal planes are the vertical plane, (variation on θ with $\rho=\infty, \phi=0.0$), and the horizontal plane, (variation on ϕ with $\rho=\infty, \theta=90.0$). In all cases, excepting the illumination-angle parameter variations, the chiral was illuminated by a plane wave, impinging from $\phi=0$ and $\theta=90$, of linear polarization, either horizontal or vertical (with respect to $\hat{\theta}$) as indicated for each case. Both the co-polarized and cross-polarized scattered fields were calculated, yielding a complete scattering matrix description of the chiral at each bistatic angle, of the form

$$\sigma(\theta, \phi) = \begin{bmatrix} HH(\theta, \phi) & HV(\theta, \phi) \\ VH(\theta, \phi) & VV(\theta, \phi) \end{bmatrix}, \quad (29)$$

which can be used to characterize the scatter for any excitation when multiplied by an appropriate transformation matrix.¹⁰ Also, the wire radius was constrained to be 0.001λ for all cases which insured the validity of the thin wire approximation.

When this study was defined, some preconceptions were held concerning what would be an optimum geometry to give an elliptically polarized scattered wave. The antenna elements comprising the chiral were expected to be of resonant dimension with the dipole being approximately one-half wavelength and the loop diameter to be determined empirically. Initially, the dipole was chosen to be exactly one-half wavelength with the loop attached at its center. With all other parameters held constant, the loop's diameter was varied from 0.001λ to 0.900λ . The resulting plots are illustrated in Figures 4 and 5. Peak scattering in all polarization states is seen to occur with the loop's diameter being approximately 0.300λ , which correlates to a circumference of approximately one wavelength, 1.000λ . With the diameter at 0.001λ , the chiral behaved essentially as a straight wire scatterer. As the loop's diameter was increased, the cross polarized component increased with the peak occurring at the loops first resonance, 0.300λ . In this regime, the chiral behaved as a polarization transformer translating a linearly polarized wave to an elliptically polarized wave. Comparing the scattered fields from both the vertical and

¹⁰ Maffet, A.L. (1968) Scattering Matrices, Chapt. 3 in *Methods of Radar Cross-Section Analysis*, New York: Academic Press, pp. 49-61.

horizontal incident polarizations, one can see they were virtually identical for a loop diameter of 0.300λ (Figures 4 and 5). This was chosen as the optimum scattering criterion. Under these conditions the electric and magnetic dipoles have approximately the same effective aperture, A_e .

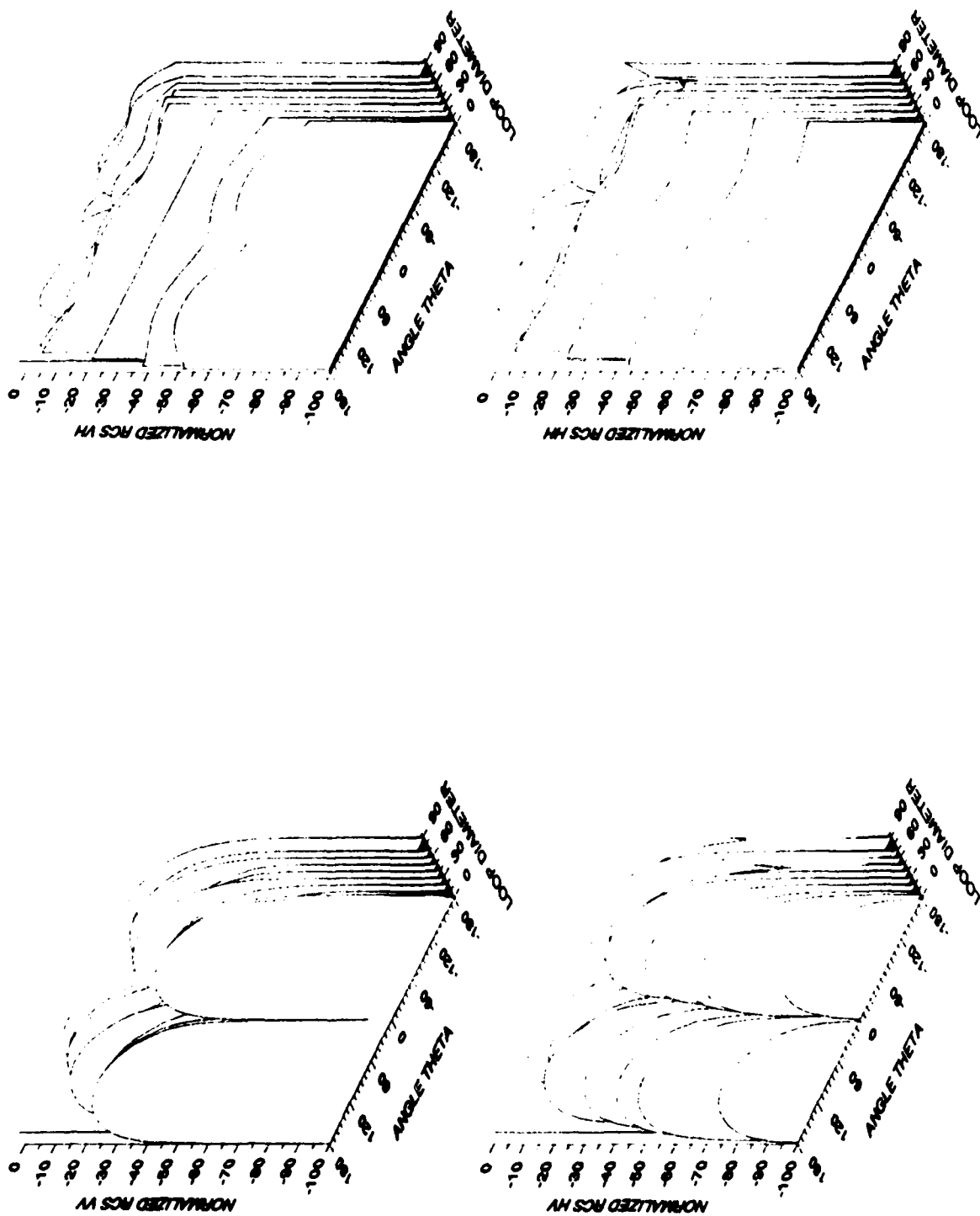


Figure 4. Loop Diameter Variation: Vertical Plane Cut Bistatic Radar Cross Section Normalized to Wavelength. The loop diameter was varied from $00.0-0.9\lambda$. (a) is σ_{VV} (b) is σ_{VH} (c) is σ_{HV} (d) is σ_{HH} .

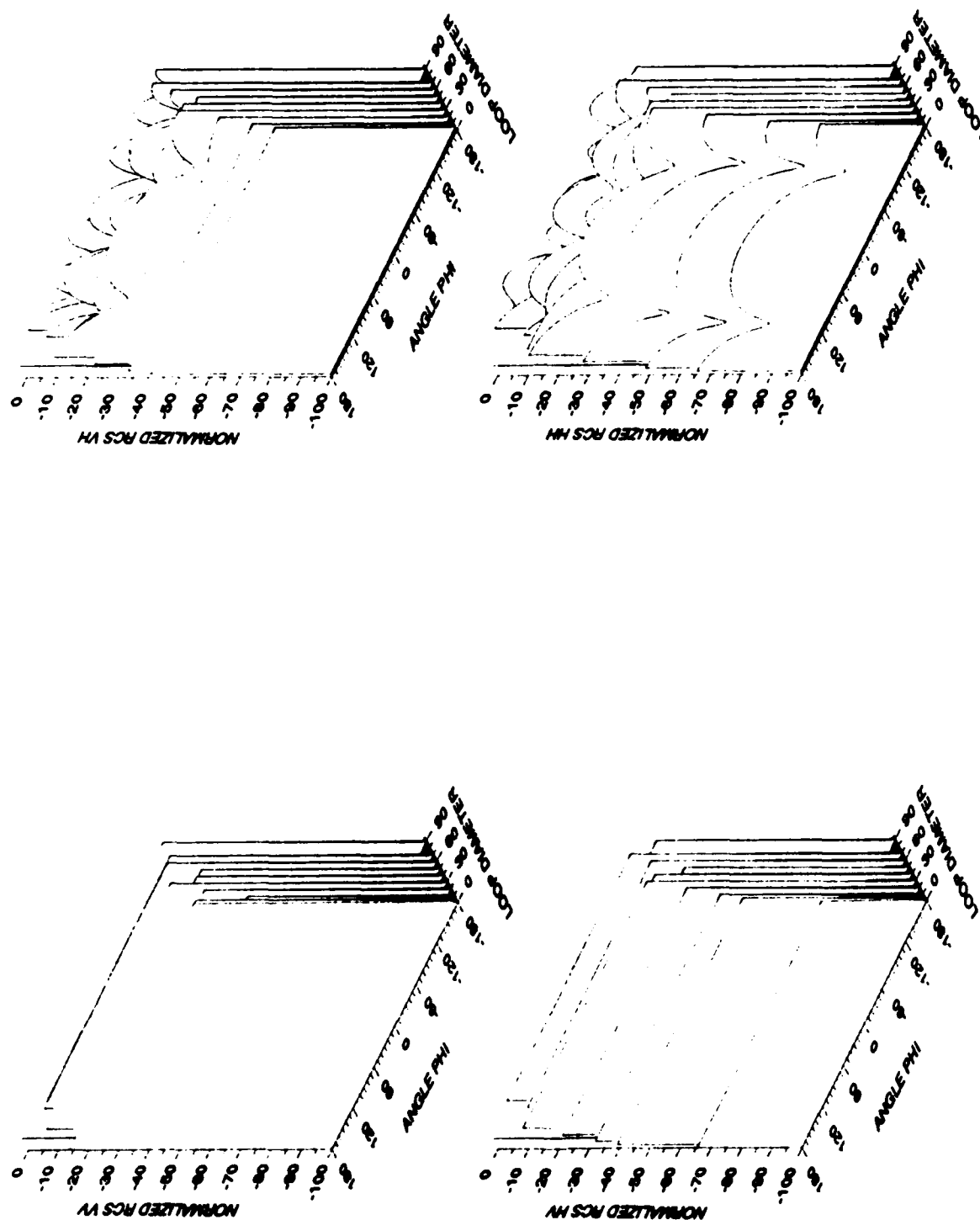


Figure 5. Loop Diameter Variation: Horizontal Plane Cut Bistatic Radar Cross Section Normalized to Wavelength. The loop diameter was varied from $0.0-0.9\lambda$. (a) is σ_{vh} (b) is σ_{vh} (c) is σ_{hv} (d) is σ_{hh} .

Having established an appropriate loop diameter, the effect of dipole length was then studied. Holding the position of the loop constant at the dipole's midpoint, the dipole's length was varied. Adjustments of the dipole's length confirmed the initial assumption that the half-wavelength dipole was an optimal choice given the equal effective aperture criterion. Figures 6 and 7 are 3-D plots of the chiral's scattering behavior as a function of dipole length. As the dipole's length is increased from 0.001λ to 0.500λ , the vertical co-polarized scattered field increased quite rapidly, while the cross-polarized term changed somewhat more slowly. This implies the dipole scattering grew quicker than the energy translated from one polarization to the other, which may also be seen in the loop diameter variations of Figures 4 and 5. Advantage may be taken of this phenomena to tailor a chiral's polarization coupling to a given design goal.

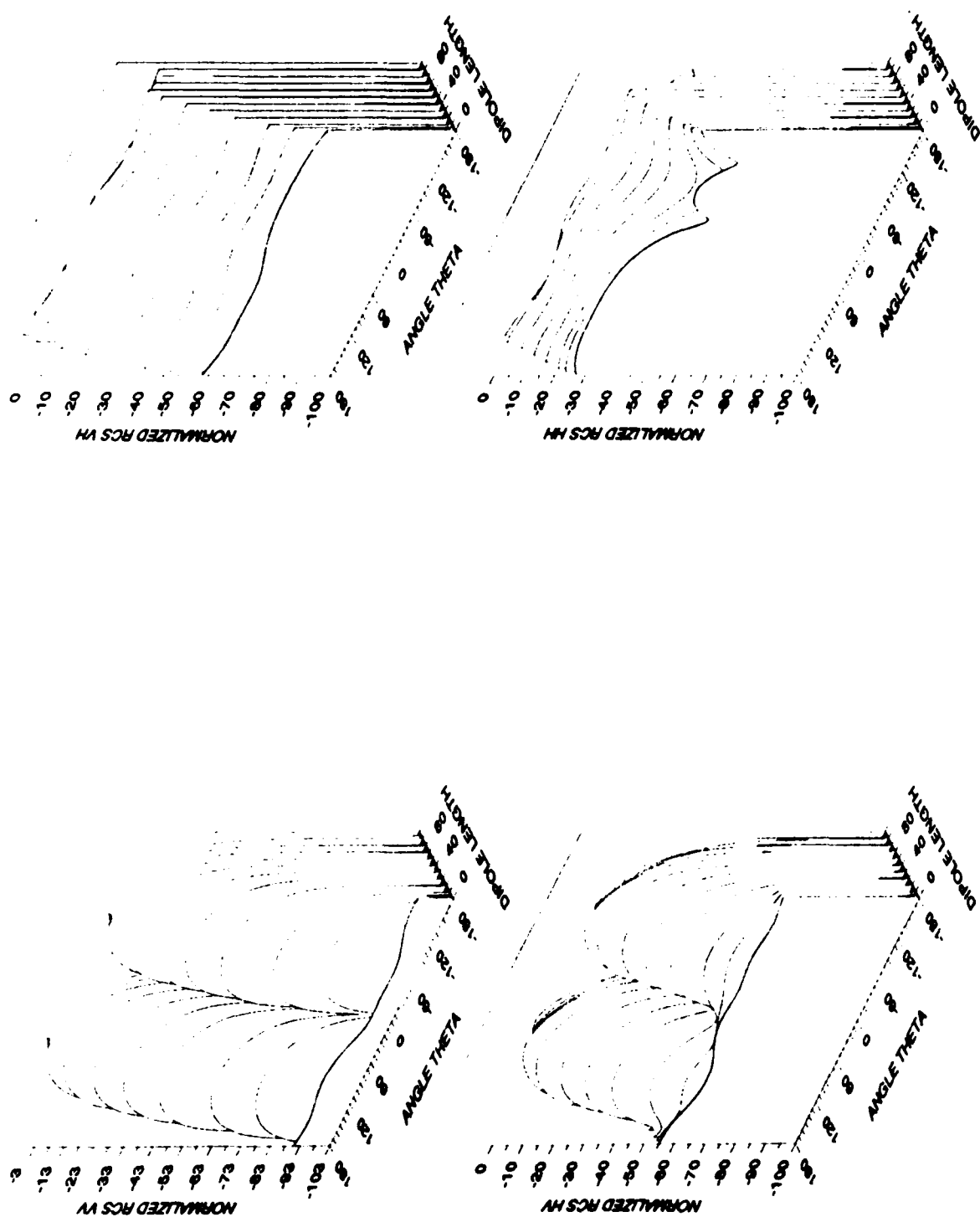


Figure 6. Dipole Length Variation: Vertical Plane Cut Radar Cross Section Normalized to Wavelength (σ/λ). The dipole's overall length was varied from 0.001λ to 0.900λ . (a) is σ_{VV} (b) is σ_{VH} (c) is σ_{HV} (d) is σ_{HH} .

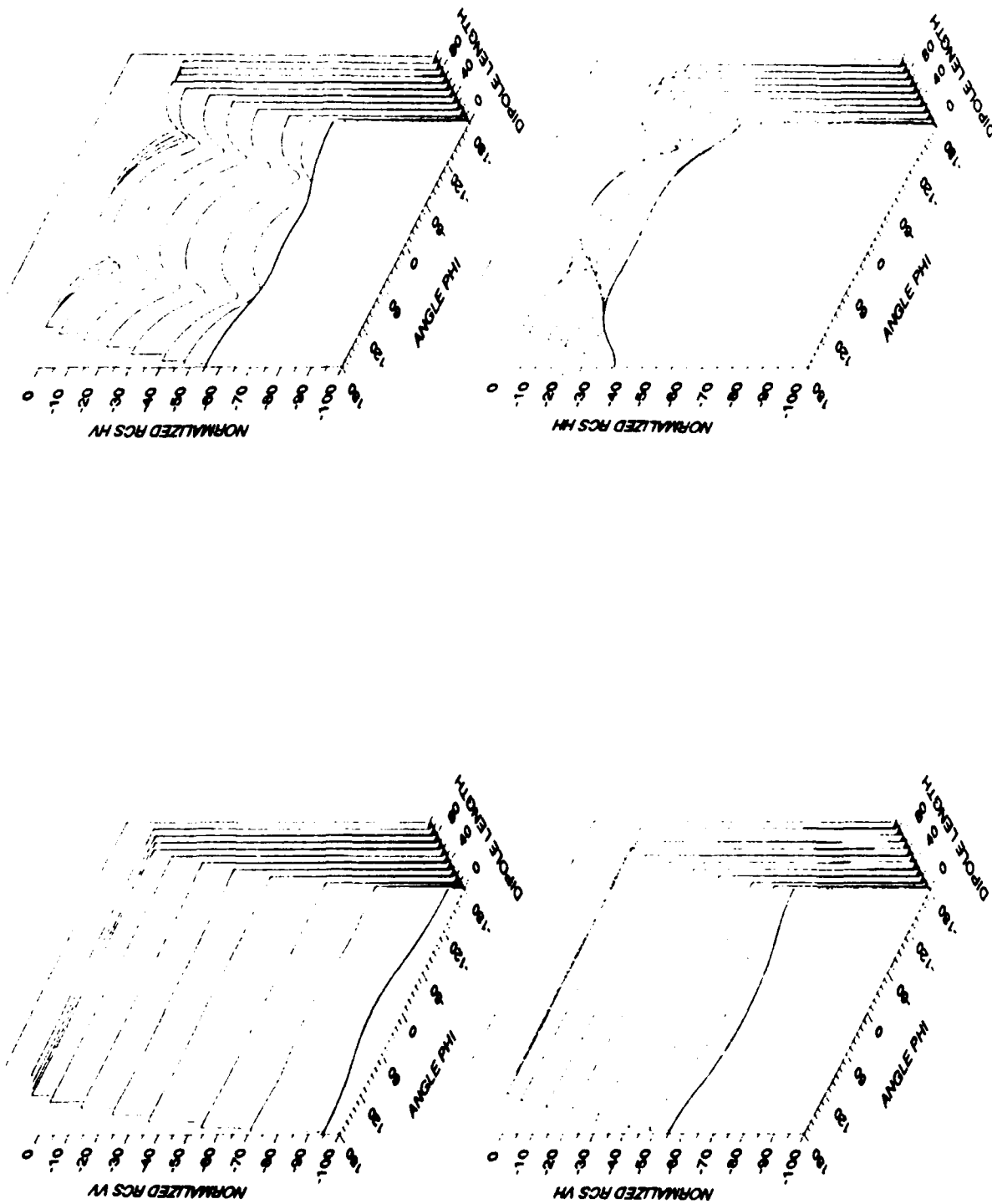


Figure 7. Dipole Length Variation: Vertical Plane Cut Radar Cross Section Normalized to Wavelength (σ/λ). The dipole's overall length was varied from 0.001λ to 0.900λ . (a) is σ_{VV} (b) is σ_{VH} (c) is σ_{HV} (d) is σ_{HH} .

With the loop and dipole dimensions fixed further parameter variations were conducted. In an attempt to improve the energy transfer from horizontal to vertical polarizations, the dipole feed point was adjusted. This would hopefully have taken advantage of the dipole input impedance dependence on feed position (dipole impedance increases with feed displacement from center). To accomplish this parameter variation, the loop's diameter and position were held constant while the upper and lower straight wire segment's lengths were adjusted. The total length of the two segments was constrained to be one-half wavelength. The resulting 3-D plot from this parameter variation is shown in Figures 8 and 9 and it indicated that both the cross and co-polarized scattered fields were reduced. This did not produce the desired effect of enhancing the polarization transformation.

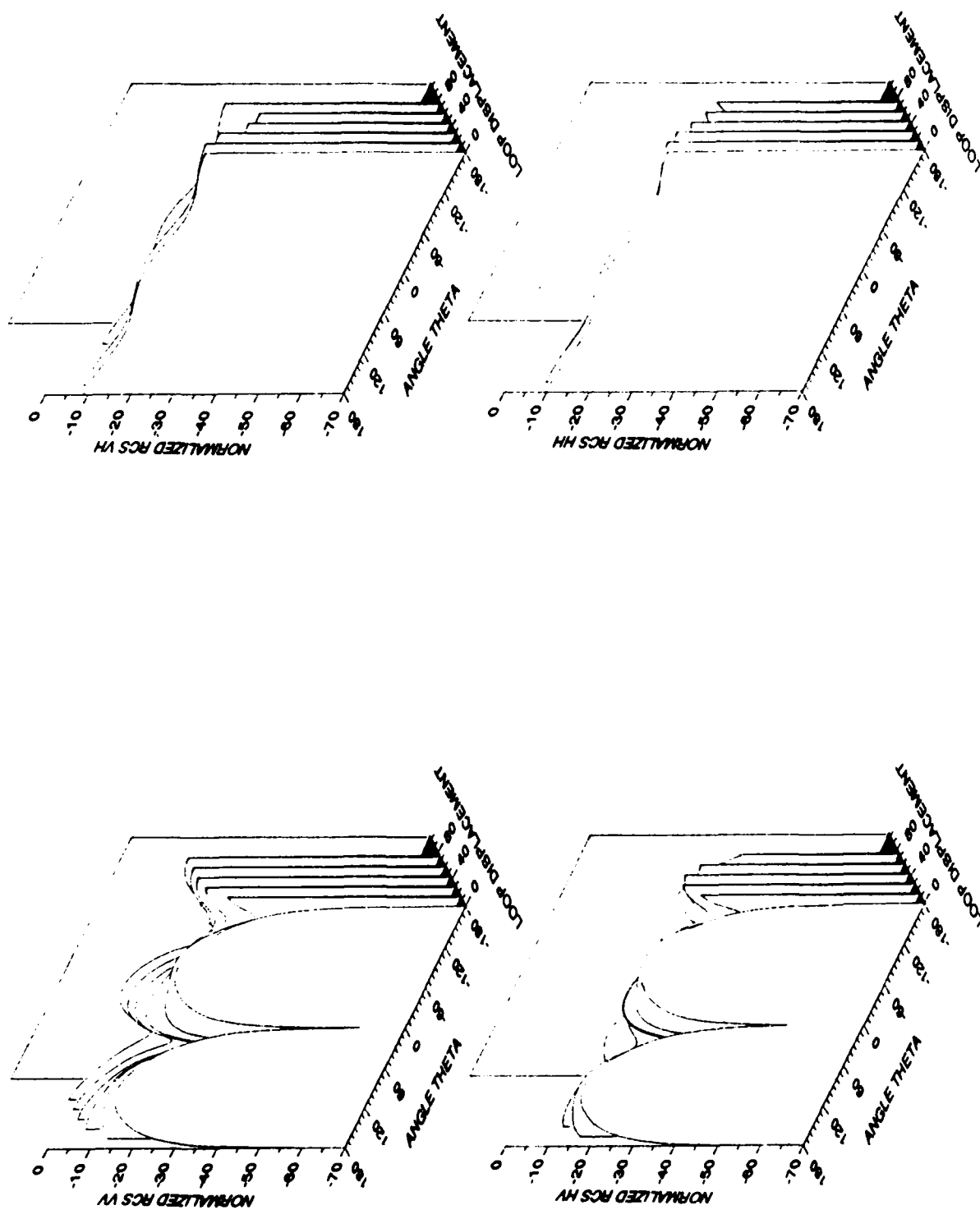


Figure 8. Dipole Feed Point Variation: Vertical Plane Cut Radar Cross Section Normalized to Wavelength (σ/λ). The dipole's feed point was displaced from the center from 0.00λ to 0.500λ . (a) is σ_{VV} (b) is σ_{VH} (c) is σ_{HV} (d) is σ_{HH} .

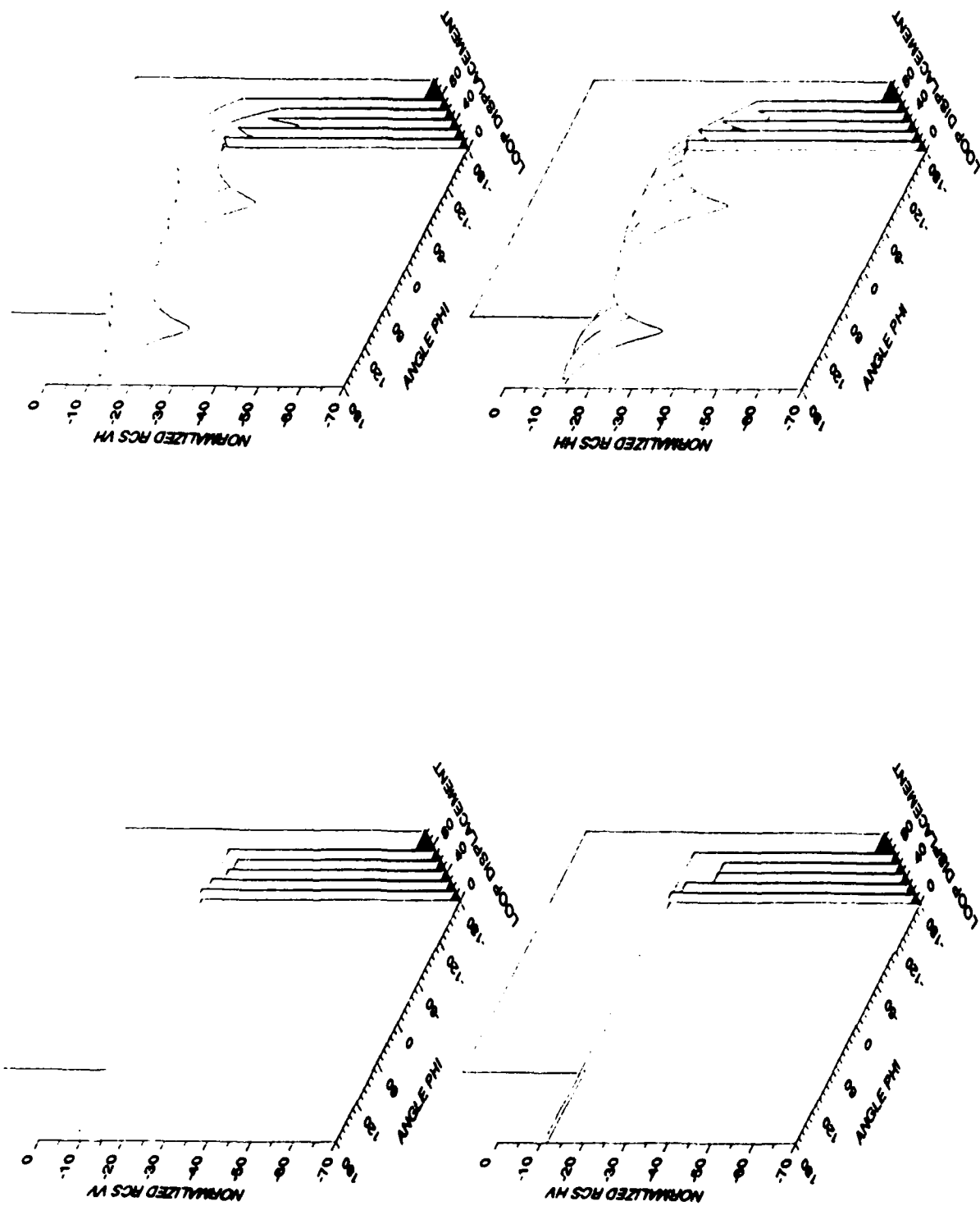


Figure 9. Dipole Feed Point Variation: Vertical Plane Cut Radar Cross Section Normalized to Wavelength (σ/λ). The dipole's feed point was displaced from the center from 0.00 λ to 0.500 λ . (a) is σ_{VH} (b) is σ_{HV} (c) is σ_{VV} (d) is σ_{HH} .

Finally, the effect of changing illumination angles was investigated. The source point was swept through both the principal planes and the scattered fields for each source angle pair were calculated. The plots of Figures 10 and 11 illustrate the chiral's behavior as theta was varied from 0 to 90 degrees and the plots of Figures 12 and 13 correspond to variation of phi from 0 to 90 degrees. From these two plots we see that the symmetries illustrated in the previous figures degenerated as theta and phi were displaced from $\phi=0$, $\theta=90$. The directional dependence of the electric and magnetic dipoles receiving patterns were responsible for some of these variations, as was expected.

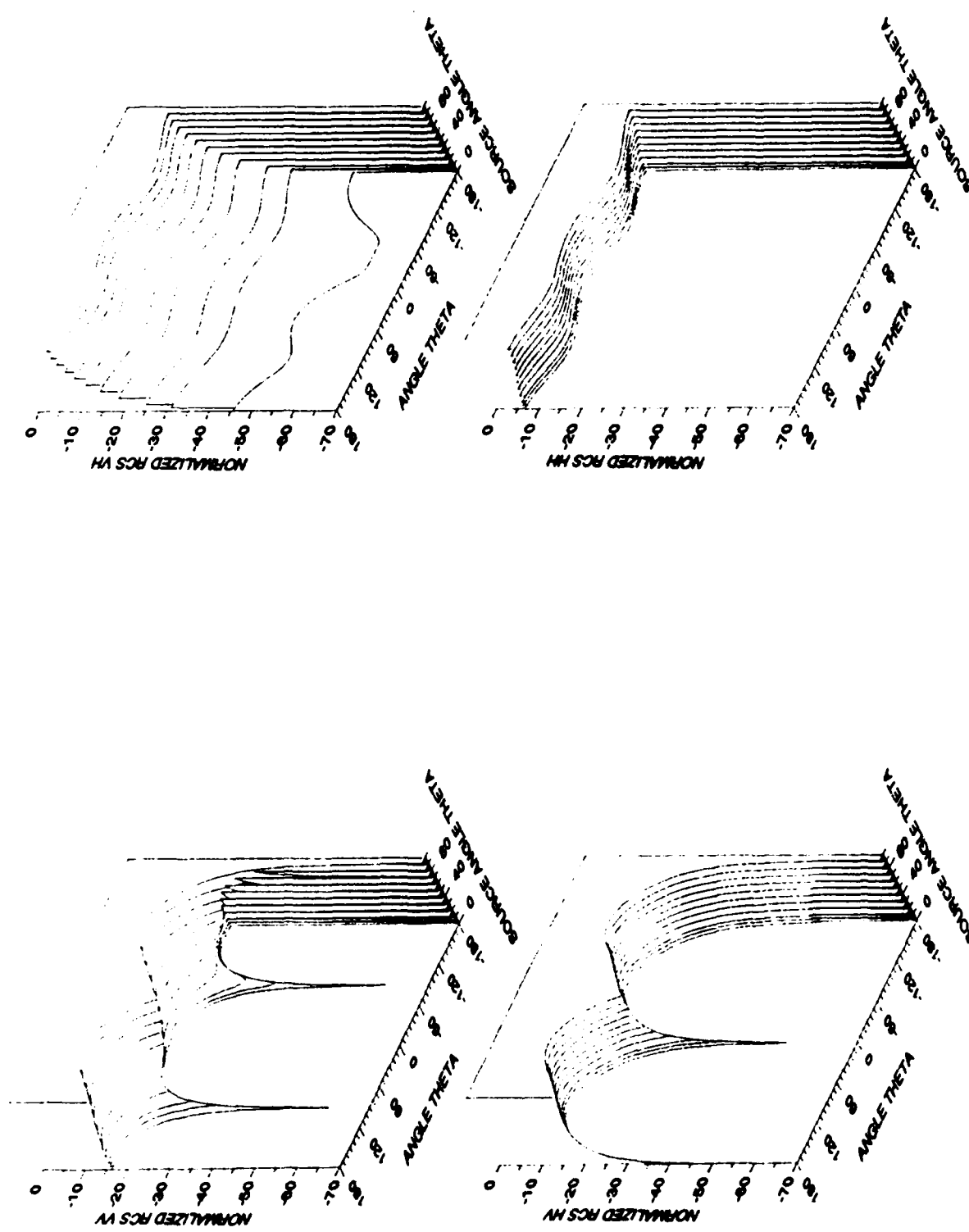


Figure 10. Illumination Angle Variation on Theta Vertical Plane Cut. Theta was varied from 0.00 to 90.0 degrees. (a) is σ_{VV} (b) is σ_{VH} (c) is σ_{HV} (d) is σ_{HH} .

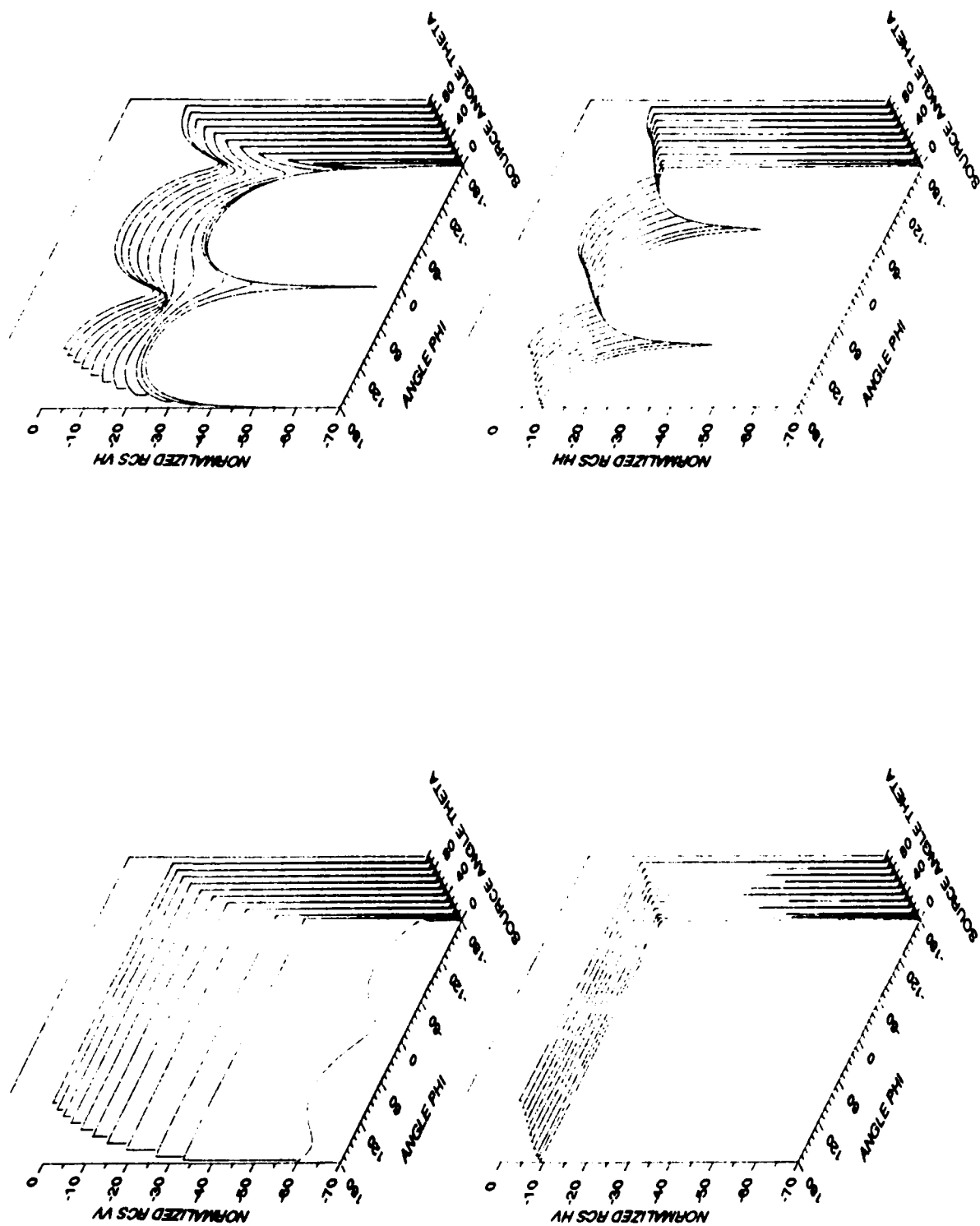


Figure 11. Illumination Angle Variation on Theta Horizontal Plane Cut. Theta was varied from 0.00 to 90.00 degrees. (a) is σ_{VV} (b) is σ_{VH} (c) is σ_{HH} (d) is σ_{HV} .

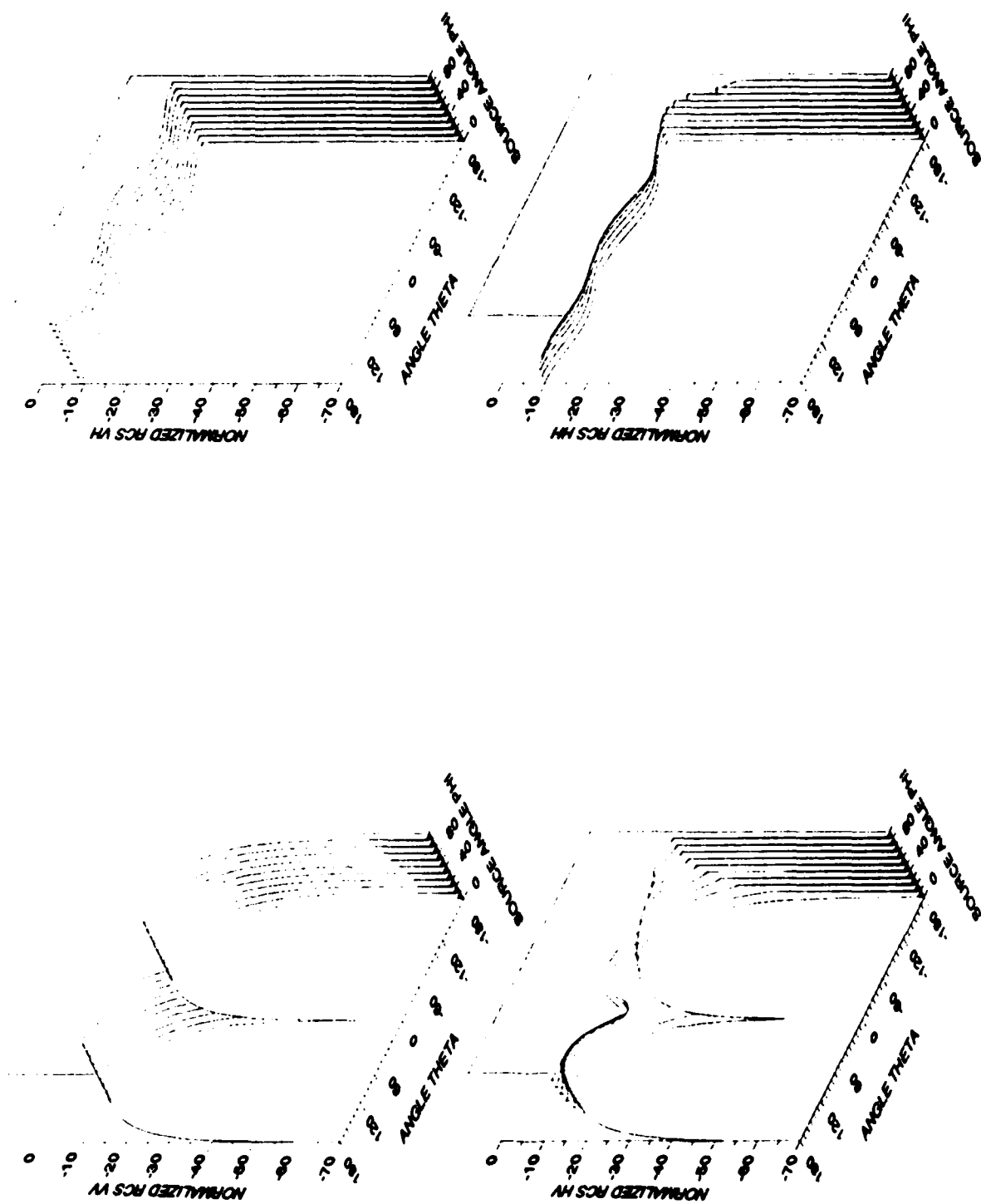


Figure 12. Illumination Angle Variation on Phi Vertical Plane Cut. Phi was varied from 0.00 to 90.00 degrees. (a) is σ_{VV} (b) is σ_{VH} (c) is σ_{HV} (d) is σ_{HH} .

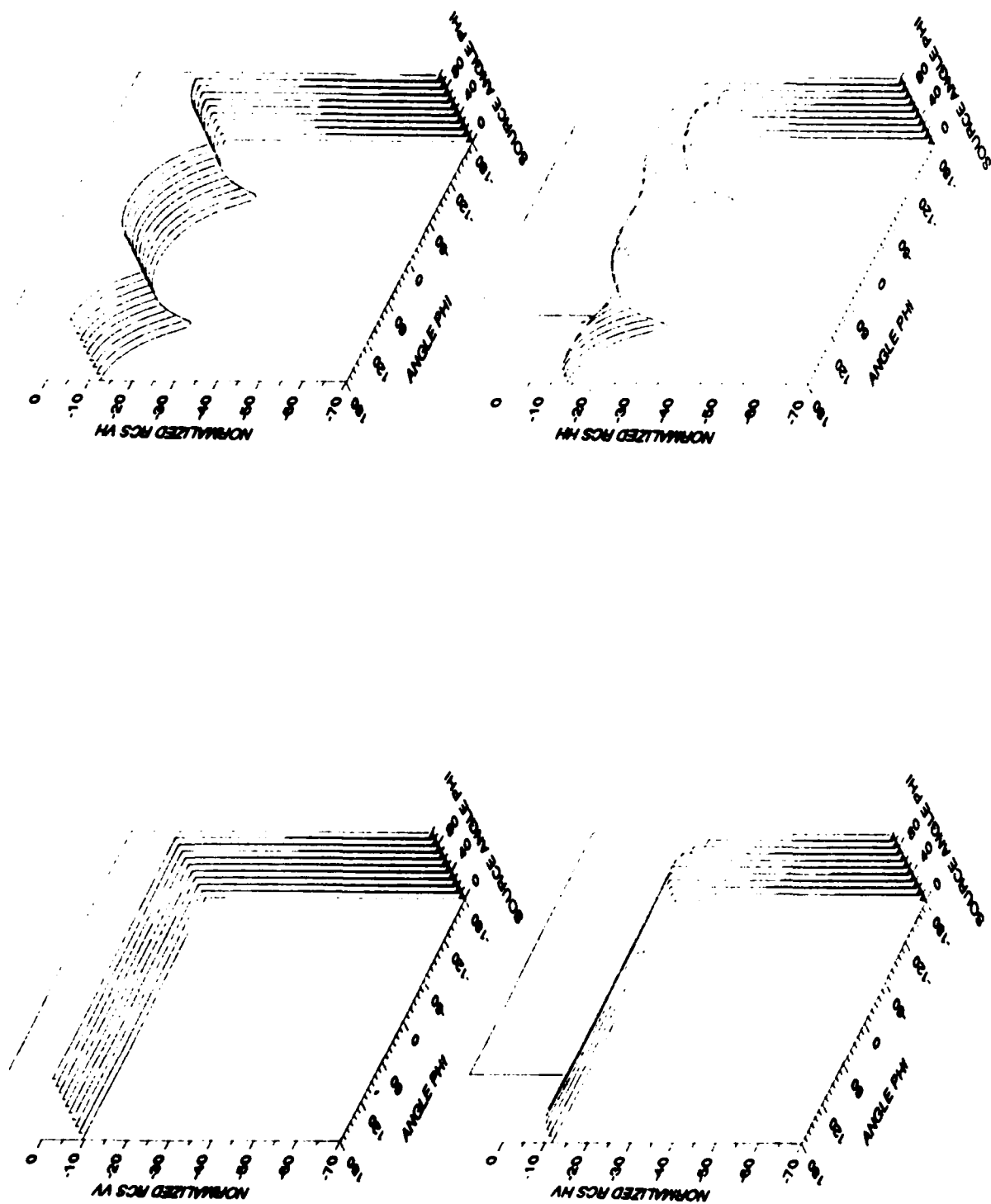


Figure 13. Illumination Angle Variation on Phi Horizontal Plane Cut. Phi was varied from 0.00 to 90.00 degrees. (a) is σ_{VV} (b) is σ_{VH} (c) is σ_{HV} (d) is σ_{HH} .

5. CONCLUSIONS

A numerical modeling system was developed and described. Included were some expectations and simple modeling techniques. The computer model performed well and appeared to be robust, provided the geometric parameters of the bent wire chiral body were within the limits of a MOM solution. Data was presented that upheld the preconceived expectations. A developmental tool, useful for studying general bent wire chirals, has been realized. This numerical modeling system will be useful to study other bent wire chiral geometries.

Future work should include studies of alternative chiral bodies. Electrically small chirals may be of use in absorbing materials and polarization rotating media. Accurate modeling of penetrable bodies, both resonant and electrically small, may yield some lightweight chirals that would be far more attractive for airborne absorbing or reflecting materials.

References

1. Jaggard, D.L., Mickelson, A.R., and Papas, C.H. (1979) On Electromagnetic Waves in Chiral Media, *Applied Physics*, New York: Springer Verlag, 18:211-216.
2. Lakhtakia, A., Varadan, V.V., and Varadan, V.K. (1986) A parametric study of microwave reflection characteristics of a planar achiral-chiral interface, *IEEE Transactions on Electromagnetic Compatibility*, EMC-28 (No. 2): 90-95.
3. Bassiri, S., Engheta, N., and Papas, C.H. (1986) Dyadic Green's function and dipole radiation in chiral media, *Alta Frequenza*, LV (No 2): 83-88.
4. Harrington, R.F. (1968) *Field Computation by Moment Methods*, Malabar, Florida: Robert E. Krieger Publishing Company, pp. 1-7.
5. Burke, G.J. and Poggio, A.J. (1980) *Numerical Electric Magnetics Code (NEC)-Method of Moments, Vol 1, Part 1*, San Diego, CA Naval Ocean Systems Command, pp. 3-5.
6. Poggio, A.J. and Miller, E.K. (1973) Integral Equation Solutions of Three Dimensional Scattering Problems, Chapt IV in *Computer Techniques for Electromagnetics*, Edited by R. Mittra, New York: Pergamon Press.
7. Harrington, R.F. (1961) *Time-Harmonic Electromagnetic Fields*, New York; McGraw-Hill Book Co.
8. Harrison, C.W. and King, R.W.P. (1969) *Antennas and Waves: A Modern Approach*, Cambridge: MIT Press, pp. 539-569.
9. Stutzman, W.L. and Thiele, G.A. (1981) *Antenna Theory and Design*, New York: John Wiley & Sons, pp. 193-203.

10. Maffet, A.L. (1968) Scattering Matrices, Chapt 3 in *Methods of Radar Cross-Section Analysis*, New York: Academic Press, pp. 49-61.



MISSION of Rome Air Development Center

RADC plans and executes research, development, test and selected acquisition programs in support of Command, Control, Communications and Intelligence (C³I) activities. Technical and engineering support within areas of competence is provided to ESD Program Offices (POs) and other ESD elements to perform effective acquisition of C³I systems. The areas of technical competence include communications, command and control, battle management information processing, surveillance sensors, intelligence data collection and handling, solid state sciences, electromagnetics, and propagation, and electronic reliability/maintainability and compatibility.